Published online 16 October 2022 *Nucleic Acids Research, 2022, Vol. 50, No. 19* **11359–11373**
https://doi.org/10.1093/nar/gkac898

Structural basis of three different transcription activation strategies adopted by a single regulator SoxS

Jing Shi [1,4,*,†], Lu Wang [1,†], Aijia Wen [3,4,†], Fulin Wang [1,†], Yuqiong Zhang [7,8,9], Libing Yu [5], Fangfang Li [1], Yuanling Jin [1], Zhenzhen Feng [1], Jiacong Li [1], Yujiao Yang [11], Fei Gao [1], Yu Zhang [1], Yu Feng [3,4,*], Shuang Wang [9,10,*], Wei Zhao [11,*] and Wei Lin [1,2,6,12,*]

[1]Department of Pathogen Biology, School of Medicine & Holistic Integrative Medicine, Nanjing University of Chinese Medicine, Nanjing 210023, China, [2]Jiangsu Collaborative Innovation Center of Chinese Medicinal Resources Industrialization, Nanjing 210023, China, [3]Department of Biophysics, Zhejiang University School of Medicine, Hangzhou 310058, China, [4]Department of Pathology of Sir Run Run Shaw Hospital, Zhejiang University School of Medicine, Hangzhou 310058, China, [5]Institute of Materials, China Academy of Engineering Physics, Mianyang 621900, China, [6]State Key Laboratory of Natural Medicines, China Pharmaceutical University, Nanjing 210023, China, [7]MOE Key Laboratory of Laser Life Science and Institute of Laser Life Science, College of Biophotonics, South China Normal University, 510631 Guangzhou, Guangdong, China, [8]Guangdong Key Laboratory of Laser Life Science, College of Biophotonics, South China Normal University, 510631 Guangzhou, Guangdong, China, [9]Songshan Lake Materials Laboratory, Dongguan 523808, Guangdong, China, [10]Beijing National Laboratory for Condensed Matter Physics, Institute of Physics, Chinese Academy of Sciences, Beijing 100190, China, [11]CAS Key Laboratory of Quantitative Engineering Biology, Shenzhen Institute of Synthetic Biology, Shenzhen Institutes of Advanced Technology, Chinese Academy of Sciences, Shenzhen 518055, China and [12]State Key Laboratory of Microbial Resources, Institute of Microbiology, Chinese Academy of Sciences, Beijing 100101, China

Received January 26, 2022; Revised September 28, 2022; Editorial Decision September 28, 2022; Accepted October 04, 2022

ABSTRACT

Transcription activation is established through extensive protein–protein and protein–DNA interactions that allow an activator to engage and remodel RNA polymerase. SoxS, a global transcription activator, diversely regulates subsets of stress response genes with different promoters, but the detailed SoxS-dependent transcription initiation mechanisms remain obscure. Here, we report cryo-EM structures of three SoxS-dependent transcription activation complexes (SoxS-TAC^{I}, SoxS-TAC^{II} and SoxS-TAC^{III}) comprising of *Escherichia coli* RNA polymerase (RNAP), SoxS protein and three representative classes of SoxS-regulated promoters. The structures reveal that SoxS monomer orchestrates transcription initiation through specific interactions with the promoter DNA and different conserved domains of RNAP. In particular, SoxS is positioned in the opposite orientation in SoxS-TAC^{III} to that in SoxS-TAC^{I} and SoxS-TAC^{II}, unveiling a novel mode of transcription activation. Strikingly, two universally conserved C-terminal domains of alpha subunit (αCTD) of RNAP associate with each other, bridging SoxS and region 4 of σ^{70}. We show that SoxS interacts with RNAP directly and independently from DNA, remodeling the enzyme to activate transcription from cognate SoxS promoters while repressing transcription from UP-element containing promoters. Our data provide a comprehensive summary of SoxS-dependent promoter architectures and offer new insights into the αCTD contribution to transcription control in bacteria.

INTRODUCTION

Regulation of transcription initiation is critical for fine-tuning of gene expression in response to changing environ-

*To whom correspondence should be addressed. Tel: +86 025 85811389; Email: weilin@njucm.edu.cn
Correspondence may also be addressed to Wei Zhao. Tel: +86 15919858900; Email: wei.zhao1@siat.ac.cn
Correspondence may also be addressed to Shuang Wang. Tel: +86 010 82649552; Email: shuangwang@iphy.ac.cn
Correspondence may also be addressed to Yu Feng. Tel: +86 0571 88208090; Fax: +86 0571 88208094; Email: yufengjay@zju.edu.cn
Correspondence may also be addressed to Jing Shi. Tel: +86 025 85811925; Email: shijing301@njucm.edu.cn
†The authors wish it to be known that, in their opinion, the first four authors should be regarded as Joint First Authors.

mental threats and generating genetic diversity across all kingdoms of life (1–4). In bacteria, canonical transcription initiation is established by the multi-subunit RNA polymerase ($\alpha_2\beta\beta'\omega\sigma$), which engages the conserved promoter elements (–35 element and –10 element), facilitates the formation of RNA polymerase-promoter closed complex (RPc), and subsequently isomerizes to a catalytically competent RNA polymerase-promoter open complex (RPo) (5–10). For non-canonical promoters that contain non-optimal consensus element, transcription is initiated by aid of various activators that associate with RNA polymerase to form activator-dependent transcription activation complexes (TACs) (11–16). As demonstrated for the classic activator catabolite activator protein (CAP or CRP), transcription activation on different promoter contexts requires distinct protein–DNA and protein–protein interactions (11,17,18). For class I promoters (such as the *lac* promoter), CAP activates transcription mainly by interacting with the CAP binding box located at the –61.5 site and the C-terminal domain of alpha subunit (αCTD) of *Escherichia coli* RNA polymerase, thereby facilitating RPc formation (15). For class II promoters (such as the *gal* promoter) that consists of a CAP binding box centered at the –41.5 site partially overlapping with the –35 element, CAP not only makes contacts with the –41.5 element, but also simultaneously interacts with αCTD, β flap, and region 4 domain of σ^{70} subunit (σ^{70}R4), thus remodeling RPc into a functional CAP-dependent transcription activation complex (CAP-TAC) ((11,15,17). However, the transcription initiation mechanisms for other promoters that harbor an activator-binding box at different locations from those of CAP (such as the –72 site positioned upstream of the –61.5 site) remain underexplored.

SoxS is the smallest member of the large AraC/XylS family transcriptional regulators. It is characterized by two conserved helix-turn-helix (HTH) DNA-binding motifs and is widely distributed in bacteria, including some dangerous human pathogens (4,18–23). As a component of the essential bacterial *soxRS* redox-sensing system, SoxS activates transcription of more than 100 functionally diverse genes involved in antibiotics resistance, oligosaccharide metabolism, and environmental threat response (21,24). SoxS-dependent promoters include the class II promoter *micF* with a SoxS-binding box (*soxbox*) centered at the –41.5 site, class I promoter *zwf* with a *soxbox* located at the –61.5 site, and an uncategorized promoter *fpr* carrying a *soxbox* positioned at the –72 site (20,25) (Figure 1A). Previous bioinformatic analysis and systematic mutagenesis showed that the *soxbox* is mainly composed of two conserved elements: recognition element A (A site, GCAC) and recognition element B (B site, CAAA) (21,26,27) (Figure 1A). Comparative analysis with the co-crystal structure of MarA in complex with *mar* DNA reveals that interactions between SoxS and *soxbox* are mainly established by two recognition helices (α3 and α6) of the two conserved HTH DNA binding motifs (27,28). It is worth noting that promoter *fpr,* which shares similar promoter context with that of *mar* DNA, harbors a SoxS binding box (*soxbox*) in the opposite orientation to that of *zwf* and *micF* (20,26,27,29,30). Although tri-alanine substitution assay subsequently inferred that SoxS might activate transcription initiation in a 'forward' or 'backward' orientation (26), the precise protein–DNA and protein–protein interactions are still elusive.

To account for the large discrepancy between numerous potential *soxbox* sites and limited SoxS molecules per cell, previous mutation analysis evidenced and supported that SoxS probably activates transcription through a 'pre-recruitment' mechanism. In pre-recruitment hypothesis, newly synthesized SoxS molecules form binary complexes with RNA polymerase in solution, then scan SoxS-dependent promoters and further activate transcription (24,25,31). Indeed, apart from SoxS–*soxbox* interactions, previous genetic and biochemical studies showed that interactions between SoxS and σ^{70}R4, and/or SoxS and αCTD are also required for SoxS-dependent transcription activation on different types of promoters (26,31–33). However, the underlying molecular mechanisms remain obscure. This raises new intriguing questions: how does such a small SoxS molecule deferentially recognize the forward and reverse promoter elements and cooperatively remodel RNA polymerase to enable flexible and efficient transcription initiation? These questions are longstanding due to the lack of structural data for SoxS-dependent transcription activation complex.

Taking SoxS as a typical model, we report cryo-EM structures of three types of intact SoxS-dependent transcription activation complex (SoxS-TAC^{I}, SoxS-TAC^{II}, and SoxS-TAC^{III}) consisting of *E. coli* RNA polymerase (RNAP), SoxS protein, and three representative SoxS-dependent promoters. These structures show that SoxS monomer regulates transcription initiation through specific interactions with the promoter DNA and different conserved domains of RNAP. Notably, SoxS is positioned in the opposite orientation in SoxS-TAC^{III} to that in SoxS-TAC^{I} and SoxS-TAC^{II}, revealing a novel mode of transcription activation. Moreover, two universally conserved C-terminal domains of RNAP alpha subunit (αCTD) synergistically cooperate with SoxS and region 4 of σ^{70} (σ^{70}R4) by their conserved distinctive determinants. These structural and biochemical data presents comprehensive architectures for SoxS-dependent transcription activation, provides a novel mode of transcription initiation mechanism, and further shed new insights on the structural diversity and generality of two RNAP αCTDs in transcription activation of bacteria.

MATERIALS AND METHODS

Plasmid construction

Plasmid pET28a-*SoxS* encoding C-terminal His6 tagged *E. coli* SoxS under the control of T7 promoter was synthesized by Sangon Biotech, Inc. Linear *micF* DNA fragment corresponding to –85 to +50 of *E. coli micF* promoter followed by Mango III coding sequencewas generated by *de novo* PCR (34–38), purified using the QIAquick PCR Purification Kit (Qiagen, Inc.), and stored at –80°C. Analogously, fragments of *zwf* DNA, *fpr* DNA, UP element DNA, and control DNA were prepared as described above. Plasmids carrying *SoxS* amino acid substitutions (pET28a-*SoxS mutants*) or *αCTD* amino acid substitutions (pREII-*NHα* mutants encodes N-terminally his-tagged *E. coli* RNAP α subunit under control of tandem *lpp* and *lacUV5* promot-

ers (39,40). were constructed using site-directed mutagenesis (QuikChange Site-Directed Mutagenesis Kit, Agilent, Inc.). Primers used in this study are shown in Supplementary Table S1.

Expression and purification of SoxS

E. coli strain BL21 (DE3) (Invitrogen, Inc.) was transformed with plasmid pET28a-*soxs* or pET28a-*soxs* derivatives. Single colonies of the resulting transformants were used to inoculate 1 l LB broth containing 50 μg/ml kanamycin, and cultures were incubated at 37°C with shaking until OD_{600} reached 0.6. Protein expression was induced by addition of IPTG to 0.5 mM, and cultures were incubated 14 h at 20°C. The cells were harvested by centrifugation (5500 × g; 15 min at 4°C), resuspended in 20 ml buffer A (20 mM Tris–HCl, pH 8.0, 0.1 M NaCl, 5% glycerol,1 mM DTT,1 mM EDTA), and lysed using an ATS AH-10013 cell disrupter (ATS, Inc.). The lysate was centrifuged (13 000 × g; 40 min at 4°C), and the supernatant was loaded onto a HiTrap Heparin HP (GE Healthcare, Inc.) equilibrated in buffer A, and the column was eluted with 120 ml linear gradient of 0.1–1 M NaCl in buffer A. Fractions containing *E. coli* SoxS were pooled and stored at –80°C. *E. coli* SoxS derivatives were expressed and purified using the same procedure as the wild type protein. PCR products of *mbp-tev-soxs* was inserted into pET28a to generate a recombinant plasmid that was used for the production of MBP-His6-TEV-SoxS. Cell pellets were harvested by centrifugation (5000 × g; 15 min at 4°C), resuspended in 20 ml lysis buffer C (50 mM Tris–HCl, pH 7.9, 0.2 M NaCl, 5% glycerol) and lysed using a JN-02C cell disrupter (JNBIO, Inc.). After being loaded onto a 5 ml column of Ni-NTA agarose (Qiagen, Inc.) equilibrated with buffer C. The column was washed with 25 ml buffer C containing 20 mM imidazole and eluted with 25 ml buffer C containing 0.20 M imidazole. Subsequently the elutes were cleaved with recombinant tobacco-etch virus protease (Life Technologies) overnight at 4°C. Then the samples were concentrated and applied to a HiLoad 16/600 Superdex 200 column (GE Healthcare, Inc.) equilibrated in buffer C, and the column was eluted with 120 ml of the same buffer. Fractions containing SoxS (without His-tag) were pooled and stored at –80 °C. Yield was ∼2.0 mg/l, and purity was >95%.

Expression and purification of *E. coli* RNAP

E. coli RNAP was prepared from *E. coli* strain BL21 (DE3) (Invitrogen, Inc.) transformed with plasmids of pGEMD (40) and pIA900 (41). Single colonies of the resulting transformants were used to inoculate 50 ml LB broth containing 100 μg/ml ampicillin, and cultures were incubated 16 h at 37 °C with shaking. Aliquots (10 ml) were used to inoculate 1 L LB broth containing 100 μg/ml ampicillin, cultures were incubated at 37°C with shaking until OD_{600} up to 0.6, cultures were induced by addition of IPTG to 1 mM, and cultures were incubated 15 h at 20°C. Then cells were harvested by centrifugation (5000 × g; 15 min at 4°C), resuspended in 20 ml lysis buffer C supplemented with 2 mM EDTA and 5 mM DTT, and lysed using a JN-02C cell disrupter (JNBIO, Inc.). After poly (ethyleneimine) precipitation and ammonium sulfate precipitation, the pellet was resuspended in buffer D (10 mM Tris–HCl, pH 7.9, 0.5 M NaCl, and 5% glycerol) and loaded onto a 5 ml column of Ni-NTA agarose (Qiagen, Inc.) equilibrated with buffer D. The column was washed with 25 ml buffer D containing 20 mM imidazole and eluted with 25 ml buffer D containing 0.15 M imidazole. The eluate was diluted in buffer E (20 mM Tris–HCl, pH 7.9, 5% glycerol, 1 mM EDTA and 1 mM DTT) and loaded onto a Mono Q 10/100 GL column (GE Healthcare, Inc.) equilibrated in buffer E and eluted with a 160 ml linear gradient of 0.3–0.5 M NaCl in buffer E. Fractions containing *E. coli* RNAP were pooled and applied to a HiLoad 16/600 Superdex 200 column (GE Healthcare, Inc.) equilibrated in buffer F (20 mM Tris–HCl, pH 8.0, 75 mM NaCl, 5 mM $MgCl_2$), and the column was eluted with 120 ml of the same buffer. Fractions containing *E. coli* RNAP were pooled and stored at –80°C. Yield was ∼2.5 mg/l, and purity was > 95%. Endogenous RNAP or its mutants containing αCTD amino acid substitutions were prepared by transforming plasmid pREII-*NHα* or pREII-*NHα* mutants into *E. coli* strain BL21 (DE3), inoculated with TB broth instead of LB broth, induced and sequentially purified as *E. coli* RNAP described above (39,40). Yield was ∼0.2 mg/l, and purities was >95%.

Assembly of *E. coli* SoxS-TAC

The full sequences of SoxS scaffolds used for cryo-EM are listed in Supplementary Table S1. Oligos were ordered gel purified from Sangon Biotech, Inc. DNA oligonucleotides scaffolds (sequences shown above) were synthesized (Sangon Biotech, Inc.) and dissolved in nuclease-free water to 1 mM. Template strand DNA and nontemplate strand DNA were annealed at 1:1 ratio in 10 mM Tris–HCl, pH 7.9, 0.2 M NaCl. Then, *E. coli* SoxS-TAC was assembled by incubating *E. coli* RNAP, *micF* scaffold (or *zwf* scaffold or *fpr* scaffold), and *E. coli* SoxS in a molar ratio of 1:1.1:15 at 4°C overnight. Subsequently, the mixture was applied to a HiLoad 16/600 Superdex 200 pg column (GE Healthcare Life Sciences) equilibrated in buffer F. After identification by SDS-PAGE and electrophoretic mobility shift assay (EMSA), the fractions containing *E. coli* SoxS-TAC were concentrated using Amicon Ultra centrifugal filters (10 kDa MWCO, Merck Millipore, Inc.).

Cryo-EM grid preparation

Immediately before freezing, 6 mM CHAPSO was added to the freshly purified *E. coli* SoxS-TAC. C-flat grids (CF-1.2/1.3–4C; Protochips, Inc.) were glow-discharged for 60 s at 15 mA prior to the application of 3 μl of *E. coli* SoxS-TAC complex, then plunge-frozen in liquid ethane using a Vitrobot (FEI, Inc.) with 95% chamber humidity at 10°C.

Cryo-EM data acquisition and processing

The grids with three types of *E. coli* SoxS-TAC were imaged using a 300 kV Titan Krios (FEI, Inc.). Images were recorded with Serial EM (41) in counting mode with a physical pixel size of 1.1 Å ($SoxS\text{-}TAC^{I}$ and $SoxS\text{-}TAC^{II}$) or 1.307 Å ($SoxS\text{-}TAC^{III}$). Data were collected with a dose of

10 e/pixel/s. Images were recorded with subframes, which were subsequently aligned and summed using MotionCor2 (42). The contrast transfer function was estimated for each summed image using CTFFIND4 (43). From the summed images, ∼10 000 particles were manually picked and subjected to 2D classification in RELION (44). 2D averages of the best classes were used as templates for auto-picking in RELION. Auto-picked particles were manually inspected, then subjected to 2D classification in RELION. Poorly populated classes were removed, resulting in a dataset of 177 709 particles. These particles were 3D-classified in RELION using a map of *E. coli* RPo (PDB ID: 6CA0) (8) low-pass filtered to 40 Å resolution as a reference. 3D classification resulted in 3 classes. Particles in Classes 3 were 3D auto-refined, and the best-resolved class containing 81 768 particles was post-processed in RELION (Supplementary Figure S3). The Gold-standard Fourier-shell- correlation analysis indicated a mean map resolution of 4.55 Å of *E. coli* SoxS-TAC^{II} (Supplementary Figure S4). Likewise, the best-resolved class containing 116 760 particles was post-processed in RELION (Supplementary Figure S5), and the Gold-standard Fourier-shell-correlation analysis indicated a mean map resolution of 3.43 Å of *E. coli* SoxS-TAC^{I} (Supplementary Figure S6). The best-resolved class containing 74 601 particles was post-processed in RELION (Supplementary Figure S7), and the Gold-standard Fourier-shell-correlation analysis indicated a mean map resolution of 4.23 Å of *E. coli* SoxS-TAC^{II} (Supplementary Figure S8).

Model building and refinement

The model of *E. coli* RNAP RPo (PDB ID: 6CA0) (8), AlphaFold predicted structure of SoxS (ID: AF-P0A9E2-F1) (45) and the ternary structure of *E. coli* MarA, DNA and RNAP αCTD (PDB ID: 1XS9) (46) were manually fitted into the cryo-EM density maps of SoxS-TAC in Coot (47), followed by adjustment of main- and side-chain conformations in Coot and real-space refinement using Phenix (48). Structures were analyzed with PyMOL (49) and Chimera (50).

In vitro transcription assay

In vitro Mango-based transcription assays were carried out by incubating *E. coli* RNAP (or endogenous *E. coli* RNAP or its derivatives), *mango* DNA (*micF* DNA, *zwf* DNA *and fpr* DNA), with or without *E. coli* SoxS or its derivatives. Transcription assay was performed in a 96-well microplate format. Reaction mixtures (80 μl) contained: 0 or 1 μM SoxS or SoxS derivatives, 0.1 μM RNAP (or 0.2 μM endogenous RNAP or its derivatives), 50 nM *mango* DNA, 1 μM TO1-Biotin, 0.1 mM NTP mix (ATP, UTP, GTP and CTP), 40 mM Tris–HCl, pH 8.0, 50 mM NaCl, 10 mM $MgCl_2$, 5% glycerol. First, *E. coli* RNAP (or endogenous RNAP or its derivatives), SoxS, and *mango* DNA were incubated for 15 min at 37 °C, then NTP mix and TO1-biotin were added into the mixture and incubated for 10 min at 37°C. Finally, fluorescence emission intensities were measured using a multimode plate reader (EnVision, PerkinElmer Inc.; excitation wavelength = 510 nm; emission wavelength = 535 nm). Relative transcription activities of SoxS derivatives were calculated using:

$$A = (I - I_0) / (I_{WT} - I_0) \quad (1)$$

where I_{WT} and I are the fluorescence intensities in the presence of SoxS and SoxS derivatives (or endogenous *E. coli* RNAP and its derivatives); I_0 is the fluorescence intensity in the absence of SoxS.

Microscale thermophoresis (MST) binding assays

His-tagged *E. coli* RNAP was labeled with the NT-647-NHS dye by using the Monolith NTTM Protein Labeling Kit RED-NHS (NanoTemper Technologies) (51–53). 250 nM of labeled RNAP were incubated with serially diluted unlabeled SoxS (without His-tag) for 15 min at room temperature in the binding buffer (1.8 mM KH_2PO_4, 10 mM Na_2HPO_4, 137 mM NaCl, 2.7 mM KCl, and 0.05% Tween-20, pH 7.8) to a final volume of 20 μl. The unlabeled proteins in each experiment were independently prepared. Then samples were loaded into NT.115 premium coated capillaries (NanoTemper Technologies). Binding experiments were performed by using the Monolith NT.115 Pico apparatus (NanoTemper Technologies) with the following parameters: LED power 5%, MST Power high. After turning on the IR-Laser, MST traces were analyzed between 4.00 and 5.00 s. and data were collected with the MO Control software version 1.6. Each fraction of the complex formed was determined by MO Affinity Analysis software version 2.3. Apparent dissociation constant (K_d) was calculated using nonlinear fitting assuming one specific binding site with the GraphPad Prism 8 software with the following formula.

$$Y = B^*_{Max} X / K_d + X \quad (2)$$

where B^*_{Max} is the maximum theoretical specific binding, here $B^*_{Max} = 1$.

Qualification and statistical analysis

For calculations of Fourier shell correlations (FSC) in Supplementary Figures S4B and E, S6B and E, S8B and E), the FSC cut-off criterion of 0.143 (54) was used. To quantify the transcription assays (Figures 2G and 3E; Supplementary S12D), mean values and the standard error of the mean from three independent measurements were calculated. The local resolution of the cryo-EM maps (Supplementary Figures S4C, S6C and S8C) was estimated using blocres (55). The quantification and statistical analyses for model refinement and validation were generated using PHENIX (48).

RESULTS

Overall structure of SoxS-TAC

To obtain different intact SoxS-TAC structures, we constructed three synthetic DNA scaffolds representing class II SoxS-dependent promoter (*micF*, from –58 to +13, positions numbered relative to the transcription start site), class

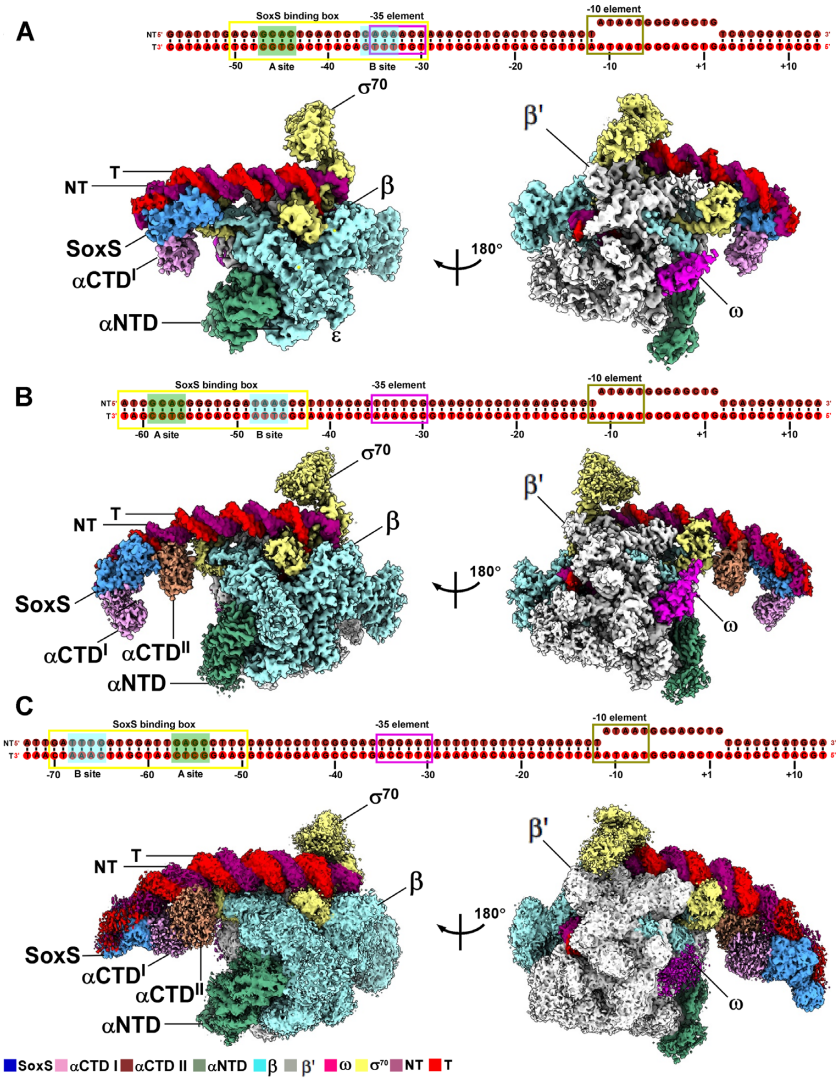

Figure 1. The overall structures of *E. coli* SoxS-TAC. (**A**) DNA scaffold used in structure determination of *E. coli* SoxS-TAC^{II} (top panel). Two views of the cryo-EM density map of *E. coli* SoxS-TAC^{II} (bottom panel). (**B**) DNA scaffold used in structure determination of *E. coli* SoxS-TAC^{I} (top panel). Two views of the cryo-EM density map of *E. coli* SoxS-TAC^{I} (bottom panel). (**C**) DNA scaffold used in structure determination of *E. coli* SoxS-TAC^{III} (top panel). Two views of the cryo-EM density map of *E. coli* SoxS-TAC^{III} (bottom panel); The EM density maps and cartoon representations of *E. coli* SoxS-TAC^{II}, *E. coli* SoxS-TAC^{I}, and *E. coli* SoxS-TAC^{III} are colored as indicated in the color key. NT, non-template-strand promoter DNA; T, template-strand promoter DNA.

I SoxS-dependent promoter (*zwf*, from –62 to +13), and a novel SoxS-dependent promoter (*fpr*, from –73 to +13) (Figure 1). Since the promoter context and transcription activation mode of *fpr* are significantly different from the previously reported classes I and II promoters (26,30), we designate it as a class III SoxS-dependent promoter. As shown in Figure 1, each of the promoter consists of a SoxS binding box *(soxbox*), a non-optimal –35 element, a consensus –10 element, a 13-nucleotide (nt) transcription bubble, and an 11-bp downstream DNA. The *soxbox* elements (containing A site and B site) differ in orientation and spacer length from the consensus –10 element. SDS-PAGE analysis of each purified complex showed that *E. coli* RNAP and *E. coli* SoxS were stoichiometrically included, indicating well-assembled SoxS-TACs (Supplementary Figure S2A). Meanwhile, we constructed three pieces of promoter DNA that carry a SoxS-dependent promoter followed by a *Mango III* sequence encoding a fluorogenic aptamer (Supplementary Figure S1) (34–38). Mango-based transcription assay showed that purified *E. coli* RNAP activates transcription on all three DNA constructs in the presence of SoxS, demonstrating the transcription activities of TACs (Supplementary Figure S2B).

We determined three intact SoxS-TAC structures using cryo-EM at nominal resolutions of 4.55 Å for SoxS-TAC^{II} (Figure 1A; Supplementary Figures S3 and S4; Table 1), 3.43 Å for SoxS-TAC^{I} (Figure 1B; Supplementary Figures S5 and S6; Table 1), and 4.23 Å for SoxS-TAC^{III} (Figure 1C; Supplementary Figures S7 and S8; Table 1). In these cryo-EM maps, the electron densities for RNAP and the

Table 1. Single particle cryo-EM data collection, processing, and model building for *E. coli* SoxS-TAC^{II}, SoxS-TAC^{I} and SoxS-TAC^{III}

	SoxS-TAC^{II}	SoxS-TAC^{I}	SoxS-TAC^{III}
Data collection and processing			
Microscope	Titan Krios	Titan Krios	Titan Krios
Voltage (kV)	300	300	300
Detector	K3 summit	K3 summit	K2 summit
Electron exposure (e/Å^2)	50	50	59
Defocus range (μm)	1.4–2.2	1.4–2.2	1.5–2.5
Data collection mode	Super resolution	Super resolution	Counting
Physical pixel size (Å/pixel)	1.1	1.1	1.307
Symmetry imposed	C1	C1	C1
Initial particle images	186 215	266 487	255 233
Final particle images	81 768	116 760	74 601
Map resolution (Å)[a]	4.55	3.43	4.23
Refinement			
Map sharpening *B*-factor (Å)	–183	–89	–104
Root-mean-square deviation			
Bond length (Å)	0.004	0.006	0.006
Bond angle (°)	0.797	0.797	0.950
MolProbity statistics	1.78	1.63	1.97
Clashscore	6.14	4.55	8.16
Rotamer outliers (%)	0.21	0.32	0.68
Cβ outliers (%)	0.0	0.0	0.0
Ramachandran plot			
Favored (%)	93.14	94.13	90.76
Outliers (%)	0.21	0.05	0.05

[a]Gold-standard FSC 0.143 cutoff criteria.

downstream DNA allowed unambiguous docking of each component and superimpose well on those of *E. coli* RPo (PDB ID: 6CA0) (8). The RNAP β' subunit consists of two coiled coils, one called clamp helices is the binding site for sigma factors and the other is called rim helices which is the binding site for Gre factors (8,56). The calculated local resolution is ∼3.0–4.5 Å for the core RNAP, and ∼5.5–7.5 Å for the peripheral αCTD and SoxS, indicating of their flexibility (Supplementary Figures S4C, S6C, S8C, S9–S11). Consistent with previous experiments (20,25,26,31,33,46), only one SoxS molecule simultaneously engages *soxbox* of the promoter DNA, αCTD, or/and σ^{70}R4 in the SoxS-TAC structures (Supplementary Figures S9C and D; S10C and D; S11C and D). As expected, SoxS interacts with *soxbox* in the same way as its homolog MarA, which inserts its two conserved HTH motifs into the corresponding DNA major grooves of *mar* binding box (PDB ID: 1BL0) (28). Likewise, in SoxS-TAC^{I} and SoxS-TAC^{II}, SoxS specifically contacts the A site and B site elements of *soxbox* with its α3 and α6 helices of the two highly conserved HTH motifs (Supplementary Figure S12A and B, left panel). Whereas, in SoxS-TAC^{III}, SoxS engages *soxbox* in the opposite direction to that of the above two structures (Supplementary Figure S12A and B, right panel). This distinct mode of interaction enables SoxS to make more interactions with RNAP and promotes RNAP remodeling.

Strikingly different from the previously reported TAC structures (11–15,38,57,58), both αCTDs (the upstream one designated as αCTD^{I} and the downstream one as αCTD^{II}) were unambiguous in the density maps of SoxS-TAC^{I} and SoxS-TAC^{III}, clearly exhibiting their distinct relative positions in the two complexes (Figure 1A and C; Supplementary Figures S5 and S7) and allowing SoxS to serve as a versatile activator.

Cryo-EM analysis of SoxS-TAC^{II} on the *micF* promoter unveils the general regulation mode for transcription activation of class II promoters

We found in our previous cryo-EM studies that the structure of a class II transcription activation complex can be more readily obtained than that of a class I complex, mainly because the former carries a conserved activator-binding box that somewhat overlaps with the consensus –35-like element in promoter DNA, and this promoter context provides more stabilizing interactions between the activator and the conserved domains of RNAP, such as αCTD, σ^{70}R4, and β flap. The *micF* promoter, which encodes a small antisense RNA involved in multidrug resistance regulation (26,59), was identified as a good example for class II SoxS-dependent promoters and was selected to assemble SoxS-TAC^{II}.

As expected, in SoxS-TAC^{II}, a single SoxS molecule contacts two conserved DNA major grooves (including A site and B site) of *soxbox* by its corresponding α3 helix (with Y33, W36, Q39 and R40) and α6 helix (with T87 and R90) from the conserved HTH motifs (Figures 1A, 2A and B; Supplementary Figure S12A and B). Our cryo-EM structure displays great similarity with the co-crystal structure of MarA in complex with its cognate DNA *mar* (PDB ID: 1BL0) with a bent upstream promoter (28), suggesting similar regulatory roles for the other SoxS/MarA-like activators of the AraC/XylS family.

Besides, SoxS simultaneously interacts with αCTD^{I} and σ^{70}R4 of RNAP. The NMR structure of *E. coli* MarA in complex with RNAP αCTD (PDB ID: 1XS9, with DNA omitted) can be well-fitted into the upstream density map of SoxS and αCTD^{I}, indicating analogous interactions between SoxS and αCTD^{I} to those between MarA and αCTD (46). Residues H3, K5, Q8, D9, A12, W13 and E16 from the

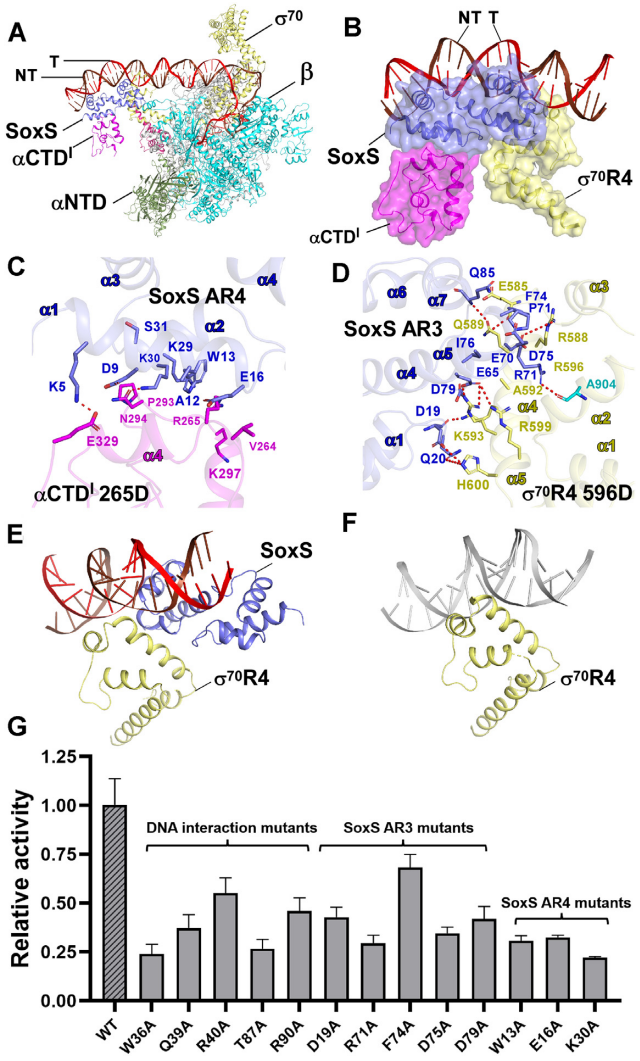

Figure 2. The critical interactions in *E. coli* SoxS-TAC^{II}. (**A**) The structure model of *E. coli* SoxS-TAC^{II}. (**B**) Relative locations of SoxS, *E. coli* RNAP αCTD^{I}, *E. coli* RNAP σ^{70}R4, and the upstream double-stranded DNA. (**C**) Detailed interactions between *E. coli* RNAP αCTD^{I} 265D and SoxS AR4. Salt-bridges are shown as red dashed lines. (**D**) Detailed interactions between *E. coli* RNAP σ^{70}R4 596D and SoxS AR3. Salt-bridges are shown as red dashed lines. (**E**) Relative locations of SoxS, *E. coli* RNAP σ^{70}R4, and the upstream double-stranded DNA. (**F**) Relative locations of *E. coli* RNAP σ^{70}R4 and the typical upstream –35 element DNA (PDB ID: 6XLL). (**G**) Substitutions of SoxS residues involved in SoxS-DNA, SoxS AR4–αCTD^{I} 265D, SoxS AR3-σ^{70}R4 596D, and SoxS AR3-β FTH interfaces decreased *in vitro* transcription activity. Data for *in vitro* transcription assays are means of three technical replicates. Error bars represent mean ± SEM of $n = 3$ experiments. Colors as in Figure 1.

α1 helix as well as K30 and S31 from the α2 helix at the N-terminal surface of SoxS mediate the above-mentioned interactions with the UP element-binding '265 determinant' of αCTD^{I} (αCTD^{I} 265D) (Figure 2A and C), the occupancy of which had been demonstrated to interfere with the transcription of UP element-containing promoters (60,61). Moreover, a cluster of residues including D19 and Q20 from the linker connecting the α1 and α2 helices, E65 from the α4 helix, F74, D75, I76, and D79 from the α5 helix, and R71 from the loop connecting the α4 and α5 helices make extensive interactions with the conserved '596 determinant' from the α4 helix of σ^{70}R4 (σ^{70}R4 596D) and the β flap tip helix (β FTH) through salt bridges, hydrogen bonds, and van der Waals forces (Figure 2D). The two involved interfaces (Figure 2C and D) share similarities with the reported transcription activator protein *T. thermophilus* TTHB099 activation region 4 (TAP AR4)- αCTD interface, the activation region 3 (TAP AR3)–σ^{70}R4 interface, and the TAP AR3–β FTH interface from the class II TAP-dependent transcription activation complex (TAP–TAC, PDB ID: 5I2D, Supplementary Figure S13A) (11). Therefore, we designate the above two exposed surfaces of SoxS as activation region 4 (SoxS AR4, Figure 2C) and activation region 3 (SoxS AR3, Figure 2D). Further comparative analysis shows that interactions between SoxS AR3 and σ^{70}R4 596D occlude σ^{70}R4 from binding to the –35 element (Figure 2E and F), in line with previous observations of biochemical assays (26). Consistently, substitution of the residues implicated in SoxS-DNA, SoxS AR4–αCTD^{I}, SoxS AR3–σ^{70}R4, and SoxS AR3–β FTH interfaces resulted in severe defects in SoxS-dependent transcription activity as identified by our Mango-based assay (Figure 2G), reflecting their necessities and biological importance.

Thus, our results and previous reports provide favorable evidences for SoxS-dependent transcription on class II promoters through a 'pre-recruitment' mechanism mediated by SoxS AR4–αCTD^{I} interactions. SoxS likely functions as a co-sigma factor to efficiently navigate RNAP from the UP element-containing or –35-like element-containing promoters to SoxS-dependent promoters.

Cryo-EM analysis of SoxS-TAC^{I} on the *zwf* promoter reveals that two αCTD cooperatively activate transcription of class I promoters

The *zwf* promoter regulates the expression of glucose-6-phosphate dehydrogenase that acts as the first essential enzyme in pentose phosphate pathway of glucose catabolism (20,26,27). It carries a *soxbox* 7 bp upstream of the –35 element (corresponding to the –61.5 site of class I CAP-dependent promoters) and is recognized as a representative class I promoter for SoxS. Growing biochemical studies have established that αCTD of *E. coli* plays an important role in CAP-dependent transcription activation, especially on class I promoters (15,33,60–62). Nevertheless, αCTD is mostly invisible in transcription activation complexes due to its high flexibility. Surprisingly, both αCTDs were visualized in our SoxS-TAC^{I} on the *zwf* promoter, bracing SoxS through different interactions and inserting their helices into the corresponding DNA major grooves similarly to that in SoxS-TAC^{II} (Figure 3A and B).

Similar to SoxS-TAC^{II}, SoxS AR4 from the α1 and α2 helices associates with the DNA-binding determinant αCTD^{I} 265D (Figures 1A, 3A and B). Meanwhile, the SoxS AR3 region (E70, R71, P72, F74, D75, I76 and D79) contacts the '287 determinant' of αCTD^{II} (αCTD^{II} 287D, including E286, V287, E288, L290 and K291) instead of σ^{70}R4 596D and β FTH in SoxS-TAC^{II} (Figure 3C). Residues E70, R71, and D75 form salt bonds with K291, E288, and E286, respectively. Hydrophobic residues P72 and I76 from SoxS as well as V287 and L290 from αCTD^{II} clus-

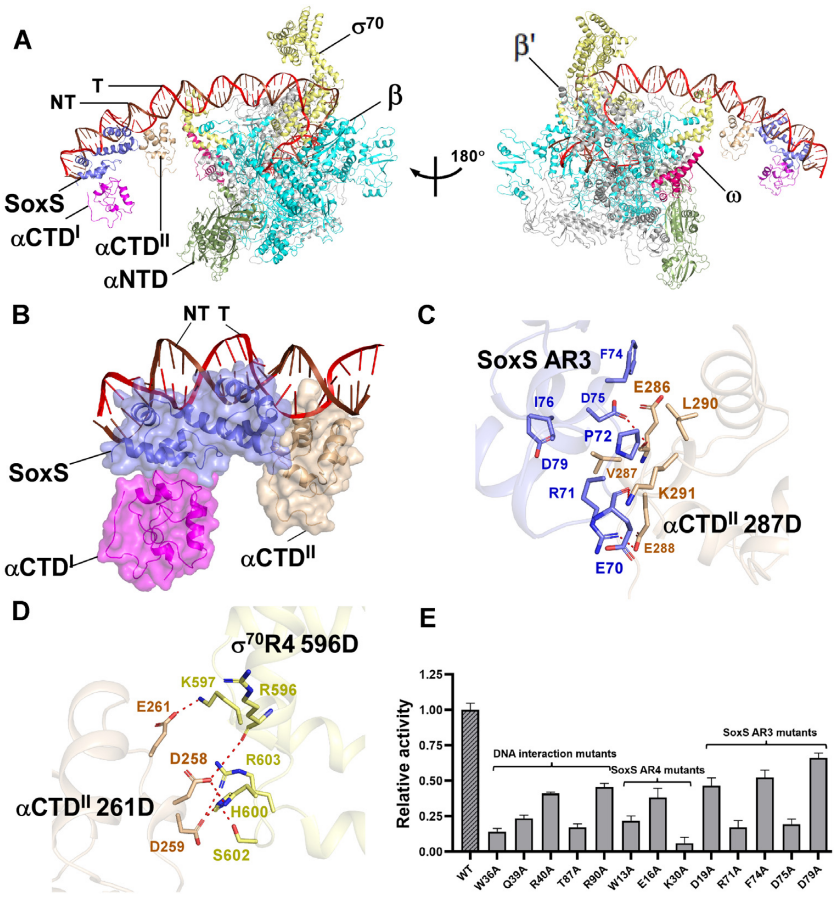

Figure 3. The critical interactions in *E. coli* SoxS-TAC^{I}. (**A**) Two views of the structure model of *E. coli* SoxS-TAC^{I}. (**B**) Relative locations of SoxS, *E. coli* RNAP αCTD^{I}, *E. coli* RNAP αCTD^{II}, and the upstream double-stranded DNA. (**C**) Detailed interactions between *E. coli* RNAP αCTD^{II} 287D and SoxS AR3. Salt-bridges are shown as red dashed lines. (**D**) Detailed interactions between *E. coli* RNAP αCTD^{II} 261D and σ^{70}R4 596D. Salt-bridges are shown as red dashed lines. (**E**) Substitutions of SoxS residues involved in SoxS-DNA, SoxS AR4–αCTD^{I} 265D and SoxS AR3–αCTD^{II} 287D interfaces decreased *in vitro* transcription activity. Colors as in Figure 1.

ter into a hydrophobic center by Van der Waals forces. Such interface resembles that between activation region 1 of CAP (CAP AR1) and αCTD from class I CAP-dependent transcription activation complex (CAP-TAC^{I}, PDB ID: 6B6H) (15), revealing the versatility of SoxS AR3 to engage different conserved domains of RNAP. Intriguingly, αCTD^{II} 265D makes conserved contacts with the UP element similar to that from CAP-TAC^{I} (Figure 3A and B; Supplementary Figure S13B), demonstrating its dual regulatory roles in mediating both protein–protein and protein–DNA interactions. In addition, the '261 determinant' of αCTD^{II} (αCTD^{II} 261D) interacts with the σ^{70}R4 596D (Figure 3D). In agreement with the above interactions, mutations of the key residues involved in SoxS-DNA, SoxS AR4–αCTD^{I} and SoxS AR3–αCTD^{II} 287D interfaces significantly reduced the transcriptional activities in Mango-based assays, implying their physiological roles (Figure 3E).

SoxS-TAC^{I} displays a similar activator-DNA-RNAP architecture to the cryo-EM structure of CAP-TAC^{I}, except for the monomeric state of SoxS and horizontally flipped conformation of αCTD^{II} (Supplementary Figure S13B). It is therefore conceivable that two αCTDs can intricately activate transcription by coordinating the interactions among the activator, the UP element DNA, and σ^{70}R4 on class I promoters.

Cryo-EM analysis of SoxS-TAC^{III} on the *fpr* promoter reveals a novel transcription activation architecture

The *fpr* promoter, which regulates the expression of an essential NADPH:ferredoxin reductase involved in the *soxRS* regulon (24), harbors a reversed *soxbox* to that of *micF* and *zwf*, while possessing a 15 bp-spacer upstream of the –35 element (26,27). Despite the challenges of analyzing a transcription complex with such a long promoter, we finally determined the cryo-EM structure of SoxS-TAC^{III} on the *fpr* promoter. In additional to the conserved SoxS-*soxbox* interaction and the αCTD^{II}-UP element interaction, SoxS-TAC^{III} presents multiple novel features.

First, in contrast to SoxS-TAC^{I} and SoxS-TAC^{II}, SoxS turns ∼180° and inserts its two conserved helices into the reversed *soxbox* element (Figures 1C, 4A and B). This finding not only agrees with previous genetic studies and docking models for SoxS and MarA (46), but also clearly defines the functional architecture of each component. Second, the backward SoxS AR4 still makes similar sets of contacts

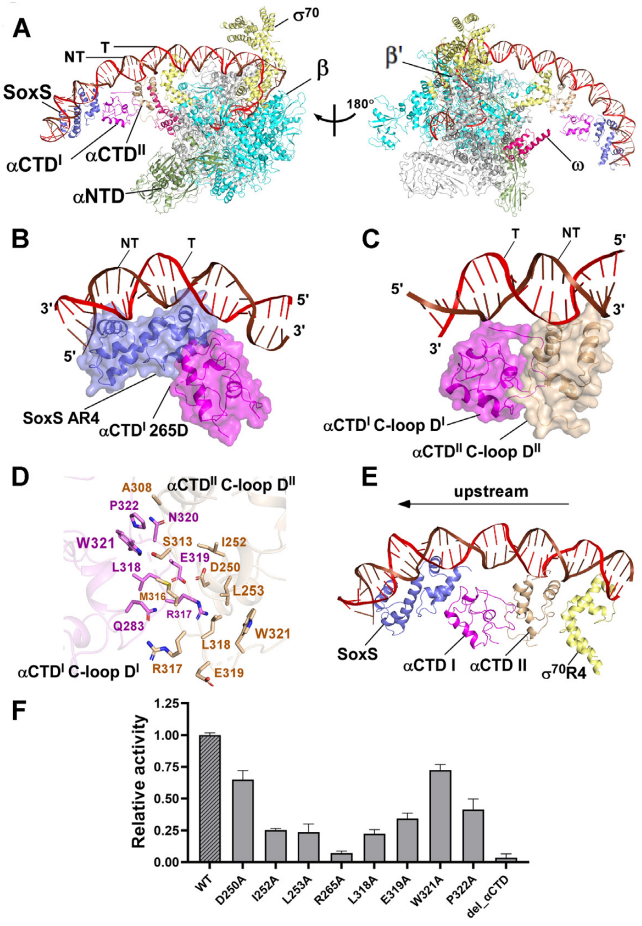

Figure 4. The critical interactions in *E. coli* SoxS-TAC^{III}. (**A**) Two views of the structure model of *E. coli* SoxS-TAC^{III}. (**B**) Relative locations of SoxS, *E. coli* RNAP αCTD^{I} 265D, SoxS AR4 and the upstream double-stranded DNA. (**C**) Relative locations of *E. coli* RNAP αCTD^{I} C-loop D^{I}, αCTD^{II} C-loop D^{II} and the upstream double-stranded DNA. (**D**) Detailed interactions between *E. coli* RNAP αCTD^{I} C-loop D^{I} and αCTD^{II} C-loop D^{II}. (**E**) Relative locations of SoxS, RNAP αCTD^{I}, αCTD^{II} and σ^{70}R4. Colors as in Figure 1. (**F**) Substitutions of αCTD residues involved in αCTD^{I} C–loop D^{I} and αCTD^{II} C–loop D^{II} interface decreased *in vitro* transcription activity.

with αCTD^{I} 265D to those in SoxS-TAC^{I} and SoxS-TAC^{II} (Figures 2C, 3B and 4B; Supplementary Figure S12A–C). Third, strikingly, both αCTD^{I} and αCTD^{II} are clearly observed and interacts with each other in SoxS-TAC^{III} (Figure 4A, C and D; Supplementary Figure S13C). Residue R317, E319, P322 from the C-terminal loop of αCTD^{I} make three hydrogen bonds with residues E319 from the C-terminal loop of αCTD^{II}, D250 from the α3 helix of αCTD^{II}, and A308 from the α4 helix of αCTD^{II}, respectively. Besides, residue L318 from the C-terminal loop of αCTD^{I} forms a hydrophobic center with I252, L253, M316 and L318 from αCTD^{II}. W321 from αCTD^{II} engages the α4 helix of αCTD^{II}, providing of stabilizing roles between the two loops. These participating residues from the C-terminal loop of αCTD^{I} form a C-loop determinant (αCTD^{I} C-loop D^{I}), and the corresponding residues in αCTD^{II} constitute a C-loop determinant (αCTD^{II} C-loop D^{II}). This loop-loop interaction serves as a bridge to connect SoxS and σ^{70}R4 across a long distance (Figure 4E), cooperatively stabilizing the conformation of SoxS-TAC^{III}. This represents a first-reported interface that mediates transcription initiation of αCTD. Fourth, the αCTD^{II} 261D interacts with the σ^{70}R4 596D in the same manner as that in SoxS-TAC^{I} (Figure 4E; Supplementary Figure S12C). In accordance with the above interactions, substitutions of the residues implicated in SoxS-DNA and SoxS AR4–αCTD^{I} interactions severely compromise SoxS-dependent transcription activity on the *fpr* promoter (Supplementary Figure S12D). In order to verify the newly identified αCTD-αCTD interactions in SoxS-TAC^{III}, we made corresponding mutations to αCTD as suggested, and successfully purified the endogenous RNAP mutants with αCTD mutations. Then we performed EMSA experiments and *in vitro* transcription assays with these RNAP mutants. Compared to wild type RNAP, RNAP mutants of W321A, P322A, D250A showed weaker bands of SoxS-TAC identified by the EMSA experiments, while I252A, L253A, R265A, L318A, E319A, del_αCTD (249–329aa) mutants displayed very weak bands of SoxS-TAC (Supplementary Figure S12E), indicating the importance of these residues in activating SoxS-TAC formation. In accordance with this, RNAP mutants of I252A, L253A, L318A, E319A confer severer defects in transcription activities than W321A, P322A and D250A. Expectedly, R265A and del_αCTD (249∼329aa) almost lost all the transcription activities (Figure 4F). These further demonstrate the αCTD–αCTD interactions in SoxS-TAC^{III} play an indispensable role in SoxS-dependent transcription activation on class III promoters.

Taken together, transcription initiation of SoxS-dependent class III promoters requires novel, αCTD-mediated protein–protein interactions to coordinate the conserved domains of an activator and RNAP. Moreover, SoxS dexterously engages the reversed promoter DNA in SoxS-TAC^{III} and provides favorable stabilizing interactions (Supplementary Figure S13D).

Comparative structural analysis of three SoxS-TAC structures supports the versatile and universal regulatory modes of RNAP αCTD in bacterial transcription activation

As mentioned above, αCTD^{I} plays essential roles in all three SoxS-TAC structures, whereas αCTD^{II} is required for transcription initiation for both class I and class III promoters with activator binding sites upstream of the –35 element. Further comparative structural analysis of the three SoxS-TAC structures demonstrates that αCTD activates transcription initiation in highly versatile modes via different determinants in different orientations.

To find out the most essential determinant for transcription activation, we superimposed and compared SoxS-TAC with different reported transcription activation complexes (aligning RNAP and DNA in the same conformation). In SoxS-TAC^{I} and SoxS-TAC^{II}, αCTD^{I} predominantly interacts with SoxS AR4 via the conserved αCTD^{I} 265D (Figure 5A, left two panels). While in SoxS-TAC^{III}, αCTD^{I} flips horizontally to make almost the same sets of interactions with SoxS AR4 (Figure 5A, middle panel), indicating the great significance of this interface for facilitating transcription initiation. Accordingly, *B. subtilis* αCTD

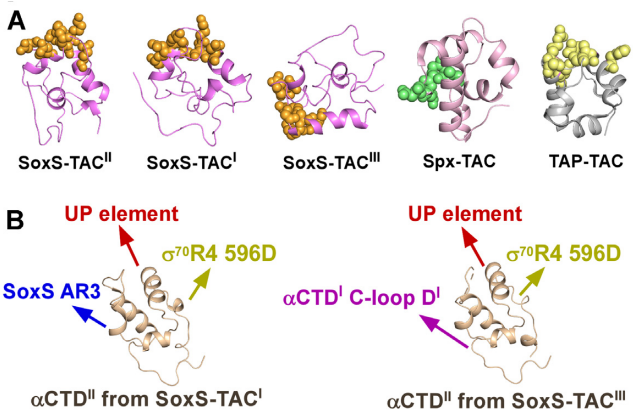

C

RNAP αCTD	Interfaces in SoxS-TAC^{II}	Interfaces in SoxS-TAC^{I}	Interfaces in SoxS-TAC^{III}
αCTD^{I}	265D-SoxS AR4	265D-SoxS AR4	265D-SoxS AR4
	/	265D-UP element	265D-UP element
αCTD^{II}	/	287D-SoxS AR3	C-loop D^{I}-C-loop D^{II}
	/	261D-σ^{70}R4 596D	261D-σ^{70}R4 596D

Note: The interfaces of SoxS AR3-σ^{70}R4 596D and SoxS AR3-β FTH are also included in SoxS-TAC^{II}.

Figure 5. RNAP αCTD exhibits versatile and universal interfaces with transcription activators in different transcription activation complexes. (**A**) RNAP αCTD exhibits versatile conformations in different transcription activation complexes. Structures of αCTD^{I} from SoxS-TAC^{II}, SoxS-TAC^{I}, SoxS-TAC^{III} are shown in cartoon with violet color, with αCTD^{I} 265D shown in orange spheres. Structures of αCTD^{I} from Spx-TAC (PDB ID: 7F75) is shown in cartoon with light pink color, with αCTD^{I} 261D shown in light green spheres. and Structures of αCTD^{I} from TAP-TAC (PDB ID: 5I2D) is shown in cartoon with light grey color, with αCTD^{I} 265D shown in light yellow spheres. (**B**) Interfaces of αCTD^{II} from SoxS-TAC^{I} (left panel) or SoxS-TAC^{III} (right panel). Arrows indicate the corresponding interaction domains from SoxS, UP element, σ^{70}R4, or αCTD^{I}. (**C**) Summary of αCTD^{I} and αCTD^{II} interfaces from SoxS-TAC^{II}, SoxS-TAC^{I} or SoxS-TAC^{III}. Colors and conformations of core RNAP and the downstream DNA are shown as in Figure 1.

from the recently reported *B. subtilis* Spx-TAC (PDB: 7F75) adopts a similar conformation to the horizontally flipped αCTD^{I}, aided by the '261D'-like helix (38) (Figure 5A, right panel). Though *T. thermophilus* αCTD from TAP-TAC (PDB ID: 5I2D) exhibits similar interactions, its conformation is turned ∼90° anticlockwise from a downward view (11) (Figure 5A, right panel). These data underscore the key roles of αCTD 265D in establishing interactions between RNAP and different activators at distinct conformations, revealing the versatility and generality properties of αCTD^{I} in bacterial transcription activation.

αCTD^{II} activates transcription through three types of contacts on class I and class III promoters. In comparison, the αCTD^{II} 265D from SoxS-TAC^{I} and SoxS-TAC^{III} make similar contacts with the corresponding DNA-binding UP element (Figure 5B, left panel; 5C). In SoxS-TAC^{I}, αCTD^{II} simultaneously interacts with SoxS AR3 and σ^{70}R4 596D by αCTD^{II} 287D and αCTD^{II} 261D, respectively (Figure 5B, left panel; 5C). These interactions strongly resemble the three corresponding interfaces involved in CAP-TAC^{I} (15) (Supplementary Figure S13B). In SoxS-TAC^{III}, apart from the αCTD^{II} 265D-UP element and αCTD^{II} 261D-σ^{70}R4 596D interactions, αCTD^{II} also interacts with αCTD^{I} via their C-loop determinants (Figure 5B, right panel; 5C). Overall, the above data emphasize the indispensable roles of these αCTD determinants in cooperative enhancement of transcription initiation.

DISCUSSION

Reversed promoters are greatly enriched in host-associated bacteria and play critical roles in regulation of genes involved in antibiotic resistance and adaptation to severe environmental perturbations. However, the underlying transcription initiation mechanism remains poorly defined. In the present study, we determined three cryo-EM structures of SoxS-TAC: class I promoter-containing SoxS-TAC^{I}, class II promoter-containing SoxS-TAC^{II}, and the reversed promoter-containing SoxS-TAC^{III}. Comparative analysis shows that a small SoxS monomer exhibits extensive interactions with the promoter DNA and the conserved domains of *E. coli* RNAP, acting as a common transcription activator on different types of promoters. Mutational analysis show that the SoxS mutants display differential defects on the different promoters, K30A, W36A, R71A, D75A, T87A, Q39A and R40A are most defective in SoxS-TAC^{I}, D79A and R90A are most defective in SoxS-TAC^{II}, while W13A, K30A, W36A, T87A, R71A, D75A confer substantial defects to all of the three types of complexes (Figure 2G, 3E and Supplementary Figure S12D), revealing their functional significance. Intriguingly, SoxS specifically interacts with the reversed *soxbox* element by its two distinctive HTH motifs in SoxS-TAC^{III}, in the opposite direction to that of SoxS-TAC^{I} or SoxS-TAC^{II}. These interactions—in combination with the stable contacts between SoxS AR4 and αCTD^{I} 265D—render αCTD^{I} sandwiched between SoxS and αCTD^{II}, which simultaneously interacts with the promoter DNA and σ^{70}R4. Positioned in an opposite orientation on the reversed promoter, SoxS greatly reduces the long distance from σ^{70}R4 and thus successfully activates transcription initiation. Notably, these elaborate 'forward-backward' activation modes of SoxS enable exceptionally stable engagement with the promoter DNA and RNAP to effectively enhance transcription activation. This novel transcription initiation mechanism may have evolutionary implications for generating genetic diversity. This unique strategy further provides favorable structural foundation for few SoxS molecules (2500 molecules per cell) to precisely discriminate *soxbox* from the abundant *soxbox*-containing promoters (65,000 SoxS binding sites per cell) *in vivo* (24,25). Since the SoxS AR4–αCTD^{I} 265D interface is identified in all three SoxS-TAC structures, it may play a crucial role in 'pre-recruitment' of SoxS *in vivo*. A number of investigations presume that ADP ribosylation on two Arg265 residues of host RNAP αCTD play an important role in bacteriophage T4-specific transcription regulation, by shutting down bacterial RNA synthesis (63–67). Nevertheless, it is more difficult to understand why the phage codes for ADP-ribosylation targeting on the second Arg265. From the structures of SoxS-TAC, we may get some hints: inactivation of two αCTD is necessary for potential efficient bacterial transcription regulation, by disrupting the αCTD-activator and αCTD-DNA interfaces.

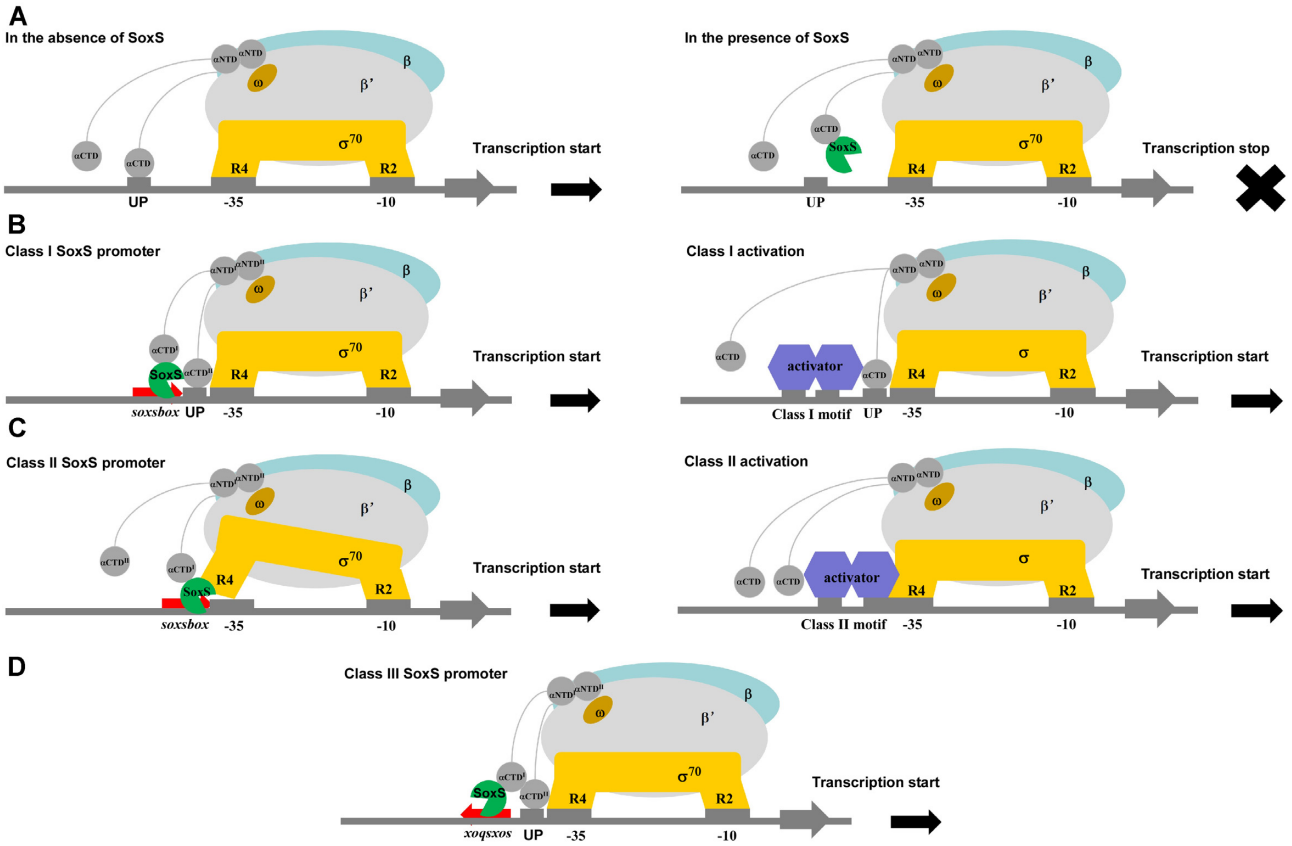

Figure 6. Proposed models for Class I/II activator-dependent and SoxS-dependent transcription activation. (**A**) Proposed working model for canonical –35/–10 element promoter-dependent transcription in the absence/presence of SoxS. (**B**) Proposed working models for Class I SoxS-dependent transcription activation (left panel) and classic Class I activator-dependent transcription activation (right panel). (**C**) Proposed working models for Class II SoxS-dependent transcription activation (left panel) and Class II activator-dependent transcription activation (right panel). (**D**) Proposed working model for Class III SoxS promoter-dependent transcription activation.

Transcription initiation is a multi-step process, activators can function at each step RNAP, from RNAP recruitment to isomerization into an active RPo to promoter escape, and promoter structures may also exhibit distinct influences. To verify the 'pre-recruitment mechanism' of SoxS proposed (24,25), we performed EMSA and MST binding assays. The EMSA experiments showed that SoxS alone displayed no detectable binding activity to different types of SoxS-dependent promoters in the presence of heparin (0.05 mg/ml). But in the presence of RNAP, stable and larger bands of SoxS-TAC formed (Supplementary Figure S14A-C), indicating that SoxS precedingly binds RNAP other than DNA. Moreover, the MST assay also showed obvious binding affinity between SoxS and RNAP in solution without DNA (Supplementary Figure S14D). In good agreement with the above and previous observations (24,26,33,46), wild type RNAP exhibits about 16.8-fold activation in the presence of SoxS in contrast to a 2.4-fold activation on the control DNA (including neither *soxsbox* nor UP element). While as to the UP element DNA, SoxS drastically reduces transcription activity to a ratio of 0.15 to that without SoxS. Expectedly, del_αCTD almost lost entire transcription activities and shows no such contrasting change (Supplementary Figure S14E). These observations along with the previous *in vivo* experiments provide more favorable evidences for the proposed 'pre-recruitment mechanism' of SoxS, in which SoxS interacts with RNAP in the absence of DNA, and diverts RNAP to transcribe properly positioned and oriented SoxS-dependent promoters. It is noteworthy that SoxS also facilitates formation of competent SoxS-TAC and most possibly acts as a pre-bound RNAP inhibitor at UP element-containing promoters. Additionally, single-molecule magnetic trap assay displayed apparent higher efficiency of promoter escape upon SoxS addition than without SoxS (Supplementary Figure S15) (68–70), suggesting a positive regulatory role of SoxS in the process of promoter escape of RNAP. From this aspect, it is presumably that SoxS activates SoxS-dependent transcription during promoter escape of RNAP transcription initiation, as well. Apart from the contributions devoted by *soxsbox* site, consensus -35 element and -10 element to SoxS-dependent activation, the different spacer length between each other on the three types of promoters may also play distinctive roles in these processes. It seems likely that the 3 bp-spacer length between -10 element and + 1 of *fpr* promoter, which consists of a lower G/C discriminator element than the other two, may differentially affects SoxS-TAC formation and promoter escape (68,70–73). And its 15 bp-spacer between *soxsbox* site and -35 element affords much more space for αCTD than a 7 bp-spacer of *zwf* pro-

moter, which probably facilitates SoxS in the 'backward' activation mode through the 'hand-in-hand' interactions between two αCTDs. However, these need to be systematically confirmed in the near future.

As noted above, our results and previous reports offer a comprehensive view of SoxS-dependent transcription regulation (Figure 6): Upon oxidative stress, cellular SoxS concentration is increased, and SoxS preferentially interacts with the DNA binding '265D' of αCTD and scans the promoters through a pre-recruitment mechanism (24,25,31). When encountering UP element-containing promoters, SoxS represses transcription by interfering with the binding domains of αCTD to the UP element (33) (Figure 6A). On class I SoxS-dependent promoter, SoxS simultaneously interacts with the *soxbox* elements and two αCTDs, remodels σ^{70}R4, assembles SoxS-TAC^{I}, and efficiently activates transcription initiation (Figure 6B). On class II SoxS-dependent promoter, SoxS-DNA, SoxS AR4–αCTD^{I}, SoxS AR3-σ^{70}R4 287D and SoxS AR3-βFTH interactions jointly promote the formation of SoxS-TAC^{II} to initiate transcription (Figure 6C). In contrast, if the scanned promoter contains a reversed *soxbox*, SoxS adopts in the opposite orientation to bind *soxbox* and presents extensive interfaces of SoxS AR4–αCTD^{I}, αCTD^{I} C-loop D^{I}-αCTD^{II} C-loop D^{II} and αCTD^{II} 261D-σ^{70}R4 596D. These interactions cooperatively facilitate SoxS-TAC^{III} formation and adaptively enhance stress gene transcription (Figure 6D). Consistent with the previous biochemical observations, it is therefore conceivable that SoxS serves as a multifunctional transcription activator that engages different classes of promoters, pre-recruits RNAP, remodels RNAP, and finally promotes DNA-melting to form transcription-competent SoxS-TAC. This study establishes an excellent example for further exploration of other transcription activators, especially for the other pathogenic AraC/XylS family members. In good agreement with our SoxS-TAC^{I} and SoxS-TAC^{II}, the most recently reported class I and class II transcription complexes of RamA also revealed similar interactions between RamA and RNAP (74), both of which uncover the importance of these interfaces in RNAP remodeling. Analogously, classic class I/II activator-dependent transcription activation models (such as CAP or TAP in dimer state) are suggested (Figure 6B and C). However, whether dimeric activator has similar class III activator-dependent transcription activation architecture to that of SoxS-TAC^{III} still needs to be discovered.

The three SoxS-TAC structures disclosed here and the previously reported transcription activation complexes provide new insights into the versatile and universal regulation roles of αCTD and σ^{70} in bacterial transcription activation (11,13,15,74). First, αCTD stabilizes transcription activation complex and promotes transcription initiation through its characteristic determinants (60,75). Both αCTD 265D and σ^{70}R4 596D play dual regulatory roles in transcription activation by mediating protein–DNA and/or protein–protein interactions (Figure 5). Second, the strategy that SoxS uses to occlude σ^{70}R4 from binding to –35 element represses the transcription of most σ^{70}-dependent genes and efficiently devotes most resources to SoxS-dependent promoters. This is reminiscent of the σ appropriation mechanism mediated by AsiA and MotA of T4 phage (12). In comparison with the results of previous biochemical assays, the interactions mediating αCTD-activator interfaces may also activate transcription by promoting the formation of RPc, while the interactions mediating αCTD-σ^{70}R4, activator-σ^{70}R4, and/or αCTD-β FTH interfaces probably activate transcription by facilitating the conversion of RPc into a competent RPo (11). Because αCTD and σ^{70}R4 are highly conserved among all bacterial RNAPs, the above mechanistic framework may also be applied to other organisms.

In addition, the above class II SoxS-dependent transcription activation mechanism shows similarities with the recently reported global transcription regulator Spx (38). Both are monomerically involved in redox homeostasis regulation, remodel specific promoter DNA and bacterial RNAP subunits to form transcription-competent activation complex, and are regulated at the post-transcriptional level by Lon protease. However, in contrast to Spx (a sensor of oxidative stress), SoxS contains no cysteine residue to act as a redox-sensing switch. Instead, it functions as a versatile stress responder. Altogether, SoxS serves as a signal amplifier by recognizing diverse types of promoters and assembling appropriate transcription initiation complexes to timely evoke target gene expression and combat environmental stresses. These versatile and intricate transcription regulation strategies may also hold good promise for engineering highly efficient and finely-tuned gene expression tools for synthetic biology.

DATA AVAILABILITY

Accession number for cryo-EM density map: EMD-32323 for SoxS-TAC^{I}, EMD-32322 for SoxS-TAC^{II}, and EMD-32324 for SoxS-TAC^{III} (Electron Microscopy Data Bank). Accession number for atomic coordinates: 7W5X for SoxS-TAC^{I}, 7W5W for SoxS-TAC^{II} and 7W5Y for SoxS-TAC^{III} (Protein Data Bank).

SUPPLEMENTARY DATA

Supplementary Data are available at NAR Online.

ACKNOWLEDGEMENTS

We appreciate Shenghai Chang at the Center of Cryo-Electron Microscopy in Zhejiang University School of Medicine and Guangyi Li, Liangliang Kong, Fangfang Wang at National Center for Protein Science, Shanghai for assistance with cryo-EM sample preparation and data collection. We thank the Core Facilities, Zhejiang University School of Medicine for technical support. We thank the Experiment Center for Science and Technology, Nanjing University of Chinese Medicine for experimental assistance. We thank Dr Zhongbo Yu (Nankai University) for helping us set up the BeadTracker software suite on our magnetic trap. *Author contributions*: J.S., L.W., A.J.W., F.L.W., Y.Q.Z., F.F.L., Y.L.J., Z.Z.F., J.C.L., Y.J.Y., F.G., Y.Z. performed the experiments. A.J.W., J.S. performed cryo-EM sample

preparations and data collections. F.Y., W.L. performed cryo-EM structure determination. J.S., F.L.W. performed biochemical experiments. J.S., W.L. designed the study, J.S., W.L., Y.F., S.W., W.Z. and L.B.Y. analyzed data, and wrote the paper.

FUNDING

National Natural Science Foundation of China [82072240, 81903756, 32270192, 32270037, 32000025]; Jiangsu Province of China [BK20190798 to W.L., BK20211302 to J.S.]; Opening Project of the State Key Laboratory of Microbial Resources, Institute of Microbiology, Chinese Academy of Sciences; Open Project of Chinese Materia Medica First-Class Discipline of Nanjing University of Chinese Medicine [2020YLXK008 to W.L., 2020YLXK016 to J.S.]; Fok Ying Tung Education Foundation; Jiangsu Specially-Appointed Professor Talent Program (to W.L.); National Natural Science Foundation of China [12004420, 32071228]; Strategic Priority Research Program of the Chinese Academy of Sciences [XDB37000000]; Youth Innovation Promotion Association of CAS [2021009]. Funding for open access charge: National Natural Science Foundation of China.
Conflict of Interest statement. None declared.

REFERENCES

1. Dorman,C.J. (1996) Flexible response: DNA supercoiling, transcription and bacterial adaptation to environmental stress. *Trends Microbiol.*, **4**, 214–216.
2. Duval,V. and Lister,I.M. (2013) MarA, SoxS and rob of *Escherichiacoli* – global regulators of multidrug resistance, virulence and stress response. *Int. J. Biotechnol. Wellness Ind.*, **2**, 101–124.
3. Decker,K.B. and Hinton,D.M. (2013) Transcription regulation at the core: similarities among bacterial, archaeal, and eukaryotic RNA polymerases. *Annu. Rev. Microbiol.*, **67**, 113–139.
4. Holden,E.R. and Webber,M.A. (2020) MarA, RamA, and SoxS as mediators of the stress response: survival at a cost. *Front. Microbiol.*, **11**, 828.
5. Feklistov,A. and Darst,S.A. (2011) Structural basis for promoter-10 element recognition by the bacterial RNA polymerase sigma subunit. *Cell*, **147**, 1257–1269.
6. Saecker,R.M., Record,M.T. and Dehaseth,P.L. (2011) Mechanism of bacterial transcription initiation: RNA polymerase-promoter binding, isomerization to initiation-competent open complexes, and initiation of RNA synthesis. *J. Mol. Biol.*, **412**, 754–771.
7. Bae,B., Feklistov,A., Lass-Napiorkowska,A., Landick,R. and Darst,S.A. (2015) Structure of a bacterial RNA polymerase holoenzyme open promoter complex. *Elife*, **4**, e08504.
8. Narayanan,A., Vago,F.S., Li,K., Qayyum,M.Z., Yernool,D., Jiang,W. and Murakami,K.S. (2018) Cryo-EM structure of *escherichia coli* sigma(70) RNA polymerase and promoter DNA complex revealed a role of sigma non-conserved region during the open complex formation. *J. Biol. Chem.*, **293**, 7367–7375.
9. Chen,J., Chiu,C., Gopalkrishnan,S., Chen,A.Y., Olinares,P.D.B., Saecker,R.M., Winkelman,J.T., Maloney,M.F., Chait,B.T., Ross,W. *et al.* (2020) Stepwise promoter melting by bacterial RNA polymerase. *Mol. Cell*, **78**, 275–288.
10. Chen,J., Boyaci,H. and Campbell,E.A. (2021) Diverse and unified mechanisms of transcription initiation in bacteria. *Nat. Rev. Microbiol.*, **19**, 95–109.
11. Feng,Y., Zhang,Y. and Ebright,R.H. (2016) Structural basis of transcription activation. *Science*, **352**, 1330–1333.
12. Shi,J., Wen,A.J., Zhao,M.X., You,L.L., Zhang,Y. and Feng,Y. (2019) Structural basis of sigma appropriation. *Nucleic Acids Res.*, **47**, 9423–9432.
13. Shi,W., Jiang,Y.N., Deng,Y.B., Dong,Z.G. and Liu,B. (2020) Visualization of two architectures in class-II CAP-dependent transcription activation. *PLoS Biol.*, **18**, e3000706.
14. Shi,J., Wen,A., Jin,S., Gao,B., Huang,Y. and Feng,Y. (2021) Transcription activation by a sliding clamp. *Nat. Commun.*, **12**, 1131.
15. Liu,B., Hong,C., Huang,R.K., Yu,Z. and Steitz,T.A. (2017) Structural basis of bacterial transcription activation. *Science*, **358**, 947–951.
16. Browning,D.F. and Busby,S.J. (2016) Local and global regulation of transcription initiation in bacteria. *Nat. Rev. Microbiol.*, **14**, 638–650.
17. Benoff,B., Yang,H., Lawson,C.L., Parkinson,G., Liu,J., Blatter,E., Ebright,Y.W., Berman,H.M. and Ebright,R.H. (2002) Structural basis of transcription activation: the CAP-alpha CTD-DNA complex. *Science*, **297**, 1562–1566.
18. Gallegos,M.T., Schleif,R., Bairoch,A., Hofmann,K. and Ramos,J.L. (1997) Arac/XylS family of transcriptional regulators. *Microbiol. Mol. Biol. Rev.*, **61**, 393–410.
19. Cortes-Avalos,D., Martinez-Perez,N., Ortiz-Moncada,M.A., Juarez-Gonzalez,A., Banos-Vargas,A.A., Estrada-de Los Santos,P., Perez-Rueda,E. and Ibarra,J.A. (2021) An update of the unceasingly growing and diverse AraC/XylS family of transcriptional activators. *FEMS Microbiol. Rev.*, **45**, fuab020
20. Li,Z. and Demple,B. (1996) Sequence specificity for DNA binding by *escherichia coli* SoxS and rob proteins. *Mol. Microbiol.*, **20**, 937–945.
21. Griffith,K.L. and Wolf,R.E. Jr (2002) A comprehensive alanine scanning mutagenesis of the *escherichia coli* transcriptional activator soxs: identifying amino acids important for DNA binding and transcription activation. *J. Mol. Biol.*, **322**, 237–257.
22. Li,T., He,L., Song,Y., Villaruz,A.E., Joo,H.S., Liu,Q., Zhu,Y., Wang,Y., Qin,J., Otto,M. *et al.* (2015) AraC-Type regulator rsp adapts *staphylococcusaureus* gene expression to acute infection. *Infect. Immun.*, **84**, 723–734.
23. Jimenez-Castellanos,J.C., Wan Ahmad Kamil,W.N., Cheung,C.H., Tobin,M.S., Brown,J., Isaac,S.G., Heesom,K.J., Schneiders,T. and Avison,M.B. (2016) Comparative effects of overproducing the arac-type transcriptional regulators MarA, SoxS, RarA and RamA on antimicrobial drug susceptibility in *klebsiellapneumoniae*. *J. Antimicrob. Chemother.*, **71**, 1820–1825.
24. Griffith,K.L. and Wolf,R.E. Jr (2004) Genetic evidence for pre-recruitment as the mechanism of transcription activation by SoxS of escherichia coli: the dominance of DNA binding mutations of soxS. *J. Mol. Biol.*, **344**, 1–10.
25. Griffith,K.L., Shah,I.M., Myers,T.E., O'Neill,M.C. and Wolf,R.E. Jr (2002) Evidence for "pre-recruitment" as a new mechanism of transcription activation in *escherichia coli*: the large excess of SoxS binding sites per cell relative to the number of SoxS molecules per cell. *Biochem. Biophys. Res. Commun.*, **291**, 979–986.
26. Zafar,M.A., Sanchez-Alberola,N. and Wolf,R.E. Jr (2011) Genetic evidence for a novel interaction between transcriptional activator SoxS and region 4 of the sigma(70) subunit of RNA polymerase at class II soxs-dependent promoters in *escherichia coli*. *J. Mol. Biol.*, **407**, 333–353.
27. Griffith,K.L. and Wolf,R.E. Jr (2001) Systematic mutagenesis of the DNA binding sites for SoxS in the escherichia coli *zwf* and *fpr* promoters: identifying nucleotides required for DNA binding and transcription activation. *Mol. Microbiol.*, **40**, 1141–1154.
28. Rhee,S., Martin,R.G., Rosner,J.L. and Davies,D.R. (1998) A novel DNA-binding motif in mara: the first structure for an AraC family transcriptional activator. *Proc. Natl. Acad. Sci. U.S.A.*, **95**, 10413–10418.
29. Fawcett,W.P. and Wolf,R.E. Jr (1994) Purification of a MalE-SoxS fusion protein and identification of the control sites of *escherichia coli* superoxide-inducible genes. *Mol. Microbiol.*, **14**, 669–679.
30. Liochev,S.I., Hausladen,A., Beyer,W.F.,Jr. and Fridovich,I. (1994) NADPH: ferredoxin oxidoreductase acts as a paraquat diaphorase and is a member of the *soxRS* regulon. *Proc. Natl. Acad. Sci. U.S.A.*, **91**, 1328–1331.
31. Zafar,M.A., Shah,I.M. and Wolf,R.E. Jr (2010) Protein-protein interactions between sigma(70) region 4 of RNA polymerase and *escherichia coli* SoxS, a transcription activator that functions by the prerecruitment mechanism: evidence for "off-DNA" and "on-DNA" interactions. *J. Mol. Biol.*, **401**, 13–32.
32. Jair,K.W., Yu,X., Skarstad,K., Thony,B., Fujita,N., Ishihama,A. and Wolf,R.E. Jr (1996) Transcriptional activation of promoters of the

superoxide and multiple antibiotic resistance regulons by rob, a binding protein of the *Escherichiacoli* origin of chromosomal replication. *J. Bacteriol.*, **178**, 2507–2513.
33. Shah,I.M. and Wolf,R.E. Jr (2004) Novel protein–protein interaction between *escherichia coli* SoxS and the DNA binding determinant of the RNA polymerase alpha subunit: SoxS functions as a co-sigma factor and redeploys RNA polymerase from UP-element-containing promoters to soxs-dependent promoters during oxidative stress. *J. Mol. Biol.*, **343**, 513–532.
34. Jeng,S.C., Chan,H.H., Booy,E.P., McKenna,S.A. and Unrau,P.J. (2016) Fluorophore ligand binding and complex stabilization of the RNA mango and RNA spinach aptamers. *RNA*, **22**, 1884–1892.
35. Autour,A., S,C.Y.J., A,D.C., Abdolahzadeh,A., Galli,A., Panchapakesan,S.S.S., Rueda,D., Ryckelynck,M. and Unrau,P.J. (2018) Fluorogenic RNA mango aptamers for imaging small non-coding RNAs in mammalian cells. *Nat. Commun.*, **9**, 656.
36. Shi,J., Gao,X., Tian,T., Yu,Z., Gao,B., Wen,A., You,L., Chang,S., Zhang,X., Zhang,Y. *et al.* (2019) Structural basis of Q-dependent transcription antitermination. *Nat. Commun.*, **10**, 2925.
37. Wang,F., Shi,J., He,D., Tong,B., Zhang,C., Wen,A., Zhang,Y., Feng,Y. and Lin,W. (2020) Structural basis for transcription inhibition by *E. coli* sspA. *Nucleic Acids Res.*, **48**, 9931–9942.
38. Shi,J., Li,F., Wen,A., Yu,L., Wang,L., Wang,F., Jin,Y., Jin,S., Feng,Y. and Lin,W. (2021) Structural basis of transcription activation by the global regulator spx. *Nucleic Acids Res.*, **49**, 10756–10769.
39. Blatter,E.E., Ross,W., Tang,H., Gourse,R.L. and Ebright,R.H. (1994) Domain organization of RNA polymerase alpha subunit: C-terminal 85 amino acids constitute a domain capable of dimerization and DNA binding. *Cell*, **78**, 889–896.
40. Niu,W., Kim,Y., Tau,G., Heyduk,T. and Ebright,R.H. (1996) Transcription activation at class II CAP-dependent promoters: two interactions between CAP and RNA polymerase. *Cell*, **87**, 1123–1134.
41. Mastronarde,D.N. (2005) Automated electron microscope tomography using robust prediction of specimen movements. *J. Struct. Biol.*, **152**, 36–51.
42. Zheng,S.Q., Palovcak,E., Armache,J.P., Verba,K.A., Cheng,Y.F. and Agard,D.A. (2017) MotionCor2: anisotropic correction of beam-induced motion for improved cryo-electron microscopy. *Nat. Methods*, **14**, 331–332.
43. Rohou,A. and Grigorieff,N. (2015) CTFFIND4: fast and accurate defocus estimation from electron micrographs. *J. Struct. Biol.*, **192**, 216–221.
44. Scheres,S.H.W. (2012) RELION: implementation of a bayesian approach to cryo-EM structure determination. *J. Struct. Biol.*, **180**, 519–530.
45. Jumper,J., Evans,R., Pritzel,A., Green,T., Figurnov,M., Ronneberger,O., Tunyasuvunakool,K., Bates,R., Zidek,A., Potapenko,A. *et al.* (2021) Highly accurate protein structure prediction with alphafold. *Nature*, **596**, 583–589.
46. Dangi,B., Gronenborn,A.M., Rosner,J.L. and Martin,R.G. (2004) Versatility of the carboxy-terminal domain of the alpha subunit of RNA polymerase in transcriptional activation: use of the DNA contact site as a protein contact site for marA. *Mol. Microbiol.*, **54**, 45–59.
47. Emsley,P. and Cowtan,K. (2004) Coot: model-building tools for molecular graphics. *Acta Crystallogr. D*, **60**, 2126–2132.
48. Adams,P.D., Afonine,P.V., Bunkoczi,G., Chen,V.B., Davis,I.W., Echols,N., Headd,J.J., Hung,L.W., Kapral,G.J., Grosse-Kunstleve,R.W. *et al.* (2010) PHENIX: a comprehensive Python-based system for macromolecular structure solution. *Acta Crystallogr. D*, **66**, 213–221.
49. Seeliger,D. and de Groot,B.L. (2010) Ligand docking and binding site analysis with PyMOL and autodock/vina. *J. Comput. Aided Mol. Des.*, **24**, 417–422.
50. Pettersen,E.F., Goddard,T.D., Huang,C.C., Couch,G.S., Greenblatt,D.M., Meng,E.C. and Ferrin,T.E. (2004) UCSF Chimera–a visualization system for exploratory research and analysis. *J. Comput. Chem.*, **25**, 1605–1612.
51. Magnez,R., Thiroux,B., Taront,S., Segaoula,Z., Quesnel,B. and Thuru,X. (2017) PD-1/PD-L1 binding studies using microscale thermophoresis. *Sci. Rep.*, **7**, 17623.
52. Welsch,M.E., Kaplan,A., Chambers,J.M., Stokes,M.E., Bos,P.H., Zask,A., Zhang,Y., Sanchez-Martin,M., Badgley,M.A., Huang,C.S. *et al.* (2017) Multivalent small-molecule Pan-RAS inhibitors. *Cell*, **168**, 878–889.
53. Jerabek-Willemsen,M., Andre,T., Wanner,R., Roth,H.M., Duhr,S., Baaske,P. and Breitsprecher,D. (2014) MicroScale thermophoresis: interaction analysis and beyond. *J. Mol. Struct.*, **1077**, 101–113.
54. Afonine,P.V., Klaholz,B.P., Moriarty,N.W., Poon,B.K., Sobolev,O.V., Terwilliger,T.C., Adams,P.D. and Urzhumtsev,A. (2018) New tools for the analysis and validation of cryo-EM maps and atomic models. *Acta Crystallogr. D Struct. Biol.*, **74**, 814–840.
55. Cardone,G., Heymann,J.B. and Steven,A.C. (2013) One number does not fit all: mapping local variations in resolution in cryo-EM reconstructions. *J. Struct. Biol.*, **184**, 226–236.
56. Vassylyeva,M.N., Svetlov,V., Dearborn,A.D., Klyuyev,S., Artsimovitch,I. and Vassylyev,D.G. (2007) The carboxy-terminal coiled-coil of the RNA polymerase beta'-subunit is the main binding site for gre factors. *EMBO Rep.*, **8**, 1038–1043.
57. Lilic,M., Darst,S.A. and Campbell,E.A. (2021) Structural basis of transcriptional activation by the *mycobacteriumtuberculosis* intrinsic antibiotic-resistance transcription factor WhiB7. *Mol. Cell*, **81**, 2875–2886.
58. Fang,C., Li,L., Zhao,Y., Wu,X., Philips,S.J., You,L., Zhong,M., Shi,X., O'Halloran,T.V., Li,Q. *et al.* (2020) The bacterial multidrug resistance regulator BmrR distorts promoter DNA to activate transcription. *Nat. Commun.*, **11**, 6284.
59. Delihas,N. and Forst,S. (2001) *MicF*: an antisense RNA gene involved in response of *escherichia coli* to global stress factors. *J. Mol. Biol.*, **313**, 1–12.
60. Busby,S. and Ebright,R.H. (1999) Transcription activation by catabolite activator protein (CAP). *J. Mol. Biol.*, **293**, 199–213.
61. Lara-Gonzalez,S., Dantas Machado,A.C., Rao,S., Napoli,A.A., Birktoft,J., Di Felice,R., Rohs,R. and Lawson,C.L. (2020) The RNA polymerase alpha subunit recognizes the DNA shape of the upstream promoter element. *Biochemistry*, **59**, 4523–4532.
62. Birch,C.A., Davis,M.J., Mbengi,L. and Zuber,P. (2017) Exploring the amino acid residue requirements of the RNA polymerase (RNAP) alpha aubunit C-Terminal domain for productive interaction between spx and RNAP of *Bacillussubtilis*. *J. Bacteriol.*, **199**, e00124-17.
63. Goldfarb,A. and Palm,P. (1981) Control of promoter utilization by bacteriophage T4-induced modification of RNA polymerase alpha subunit. *Nucleic Acids Res.*, **9**, 4863–4878.
64. Kassavetis,G.A., Elliott,T., Rabussay,D.P. and Geiduschek,E.P. (1983) Initiation of transcription at phage T4 late promoters with purified RNA polymerase. *Cell*, **33**, 887–897.
65. Geiduschek,E.P. (1991) Regulation of expression of the late genes of bacteriophage t4. *Annu. Rev. Genet.*, **25**, 437–460.
66. Koch,T., Raudonikiene,A., Wilkens,K. and Ruger,W. (1995) Overexpression, purification, and characterization of the ADP-ribosyltransferase (gpAlt) of bacteriophage T4: ADP-ribosylation of e. coli RNA polymerase modulates T4 "early" transcription. *Gene Expr.*, **4**, 253–264.
67. Wilkens,K., Tiemann,B., Bazan,F. and Ruger,W. (1997) ADP-ribosylation and early transcription regulation by bacteriophage t4. *Adv. Exp. Med. Biol.*, **419**, 71–82.
68. Revyakin,A., Ebright,R.H. and Strick,T.R. (2004) Promoter unwinding and promoter clearance by RNA polymerase: detection by single-molecule DNA nanomanipulation. *Proc. Natl. Acad. Sci. U.S.A.*, **101**, 4776–4780.
69. Lerner,E., Chung,S., Allen,B.L., Wang,S., Lee,J., Lu,S.W., Grimaud,L.W., Ingargiola,A., Michalet,X., Alhadid,Y. *et al.* (2016) Backtracked and paused transcription initiation intermediate of *escherichia coli* RNA polymerase. *Proc. Natl. Acad. Sci. U.S.A.*, **113**, E6562–E6571.
70. Hook-Barnard,I.G. and Hinton,D.M. (2007) Transcription initiation by mix and match elements: flexibility for polymerase binding to bacterial promoters. *Gene Regul Syst Bio*, **1**, 275–293.
71. Aoyama,T., Takanami,M., Ohtsuka,E., Taniyama,Y., Marumoto,R., Sato,H. and Ikehara,M. (1983) Essential structure of *e. coli* promoter: effect of spacer length between the two consensus sequences on promoter function. *Nucleic Acids Res.*, **11**, 5855–5864.
72. Hook-Barnard,I.G. and Hinton,D.M. (2009) The promoter spacer influences transcription initiation via sigma70 region 1.1 of *escherichia coli* RNA polymerase. *Proc. Natl. Acad. Sci. U.S.A.*, **106**, 737–742.

73. Winkelman,J.T., Chandrangsu,P., Ross,W. and Gourse,R.L. (2016) Open complex scrunching before nucleotide addition accounts for the unusual transcription start site of e. coli ribosomal RNA promoters. *Proc. Natl. Acad. Sci. U.S.A.*, **113**, E1787–E1795.
74. Hao,M., Ye,F., Jovanovic,M., Kotta-Loizou,I., Xu,Q., Qin,X., Buck,M., Zhang,X. and Wang,M. (2022) Structures of class i and class II transcription complexes reveal the molecular basis of rama-dependent transcription activation. *Adv. Sci. (Weinh)*, **9**, e2103669.
75. Igarashi,K. and Ishihama,A. (1991) Bipartite functional map of the *E. coli* RNA polymerase alpha subunit: involvement of the C-terminal region in transcription activation by cAMP-CRP. *Cell*, **65**, 1015–1022.